Transport properties of one-dimensional Kronig - Penney models with correlated disorder

1997 J. Phys.: Condens. Matter 9 1777

(http://iopscience.iop.org/0953-8984/9/8/009)

J. Phys.: Condens. Matter **9** (1997) 1777–1791. Printed in the UK PII: S0953-8984(97)77366-1

Transport properties of one-dimensional Kronig–Penney models with correlated disorder

Tsampikos Kottos†, G P Tsironis† and Felix M Izrailev†‡§

† Department of Physics, University of Crete and Research Centre of Crete, PO Box 1527, 71110 Heraklion, Crete, Greece

‡ Budker Institute of Nuclear Physics, Novosibirsk 630090, Russia

Received 27 August 1996, in final form 24 October 1996

Abstract. Transport properties of one-dimensional Kronig–Penney models with binary correlated disorder are analysed using an approach based on classical Hamiltonian maps. In this method, extended states correspond to bound trajectories in the phase space of a parametrically excited linear oscillator, while the on-site potential of the original model is transformed to an external force. We show that in this representation the two-probe conductance takes a simple geometrical form in terms of evolution areas in phase space. We also analyse the case of a general N-mer model.

1. Introduction

The random-dimer model, a tight-binding model with correlated disorder, introduced in references [1, 2], has attracted considerable attention due to the presence of transparent states in an otherwise disordered one-dimensional system [1–9]. In the present paper we address the issue of the spectrum of the random-dimer Kronig–Penney (RDKP) model [10] and extensions using the same Hamiltonian approach as was applied earlier in the context of tight-binding models [9]. Using techniques from dynamical systems theory [11], we construct a Poincaré map that turns the Kronig–Penney model into an equivalent tight-binding model, and study the latter through a two-dimensional map corresponding to a classical linear oscillator with a parametric perturbation given in the form of periodic δ-kicks [9]. The amplitudes of these kicks are defined by the site potential of the tight-binding model. In this representation, extended states of the tight-binding model are represented through bounded trajectories in the phase space of the Hamiltonian map. Furthermore, in this representation the two-probe conductance is related to the time evolution (under the Hamiltonian map) of areas initially defined by the basis unit vectors. This new approach provides an effective and simple tool for use in achieving an understanding of transport properties, and the structure of eigenstates, as well as for deriving analytical expressions. In particular, one can easily determine fully transparent states for the general case where N sites are correlated.

In the following section we summarize briefly the Hamiltonian map approach used in reference [9], and apply it in the context of the RDKP model. In section 3 we analyse transport properties through a new expression for conductance, while in section 4 we give our conclusions.

§ E-mail addresses: izrailev@vxinpb.inp.nsk.su; izrailev@physics.spa.umn.edu.

0953-8984/97/081777+15$19.50

2. The Hamiltonian map approach

2.1. The time-dependent linear map

The model of interest is the one-dimensional Schrödinger equation with an array of δ-function potentials:

$$E\phi(z) = -\frac{\mathrm{d}^2\phi(z)}{\mathrm{d}z^2} + \sum_{n=1}^{L} \epsilon_n \delta(z - z_n)\phi(z). \tag{1}$$

Equation (1) defines the Kronig–Penney model, where E is the eigenenergy of the stationary states, ϵ_n is the strength of the potential, and z denotes the space, while we take the positions of the δ-functions to be regularly spaced ($z_n = n$). The tight-binding model corresponding to equation (1) is [11]

$$\phi_{n+1} + \phi_{n-1} = v_n \phi_n \qquad v_n = 2\cos(q) + \epsilon_n \frac{\sin(q)}{q} \tag{2}$$

with $q^2 \equiv E$, $\phi_n \equiv \phi(z = n)$; equation (2) can be written equivalently as a two-dimensional map M_n, i.e.

$$\begin{pmatrix} x_{n+1} \\ y_{n+1} \end{pmatrix} = \begin{pmatrix} v_n & -1 \\ 1 & 0 \end{pmatrix} \begin{pmatrix} x_n \\ y_n \end{pmatrix} \tag{3}$$

where $\phi_n = x_n$ and $y_n = \phi_{n-1}$. An eigenstate of equation (2) is a 'trajectory' of the map of equation (3). Straightforward diagonalization of this map leads to the eigenvalues

$$\lambda_n^{\pm} = \frac{v_n \pm \mathrm{i}\sqrt{4 - v_n{}^2}}{2} = \mathrm{e}^{\pm \mathrm{i}\mu_n}$$

where the phase μ_n is introduced by the relation $v_n = 2\cos\mu_n$. For $|v_n| < 2$ we obtain a stable map rotation with phase μ_n. For $|v_n| = 2$ we find the curves separating regions of allowed and forbidden energies, determined through the equations $q = (2k+1)\pi$, for $\epsilon = -2q\cot(q/2)$, and $q = 2k\pi$, for $\epsilon = 2q\tan(q/2)$, with $k = 0, 1, 2, \ldots$. To understand the origin of the resonant states in the RDKP model resulting when adjacent pairs of random energies ϵ_n coincide [10], we consider the sequence ϵ_n which consists of one dimer only, i.e. where all of the values of ϵ_n are equal to ϵ_1 except two values for which we have $\epsilon_m = \epsilon_{m+1} = \epsilon_2$. From the property of the map eigenvalues found previously we observe that this unique dimer with energy ϵ_2 does not influence the trajectories of the map of equation (3) when the total phase advance $\mu_m + \mu_{m+1} = 2\mu_m$ through the dimer is equal to π or 2π. Since the latter value $\mu_m = \pi$ is forbidden, from the stability conditions, the resonant energy $q_{cr}^2 \equiv E_{cr}$ is defined by $\mu_m = \pi/2$ giving $-2q_{cr}/\epsilon_2 = \tan(q_{cr})$. As a result, for the general case of randomly distributed dimers ϵ_1 and ϵ_2, there are two resonant values:

$$q_{cr} = -\frac{\epsilon_{1,2}\tan(q_{cr})}{2} \tag{4}$$

for which dimers of the first type, ϵ_1, or of the second, ϵ_2, have no influence on the transparent states. One should note that since $\tan(q_{cr})$ is a π-periodic function and takes values in $(-\infty, +\infty)$, we have an infinite set of critical energies q_{cr} (two in every interval $[(2k-1)\pi/2, (2k+1)\pi/2]$) [10]. However, for the first allowed band defined through the condition $|v_n| = 2$, the disorder strength ϵ must be greater than a critical value $\epsilon_{cr} = -2$ in order to have resonant states. The critical disorder for reflectionless modes to appear arises only in the first band of the spectrum.

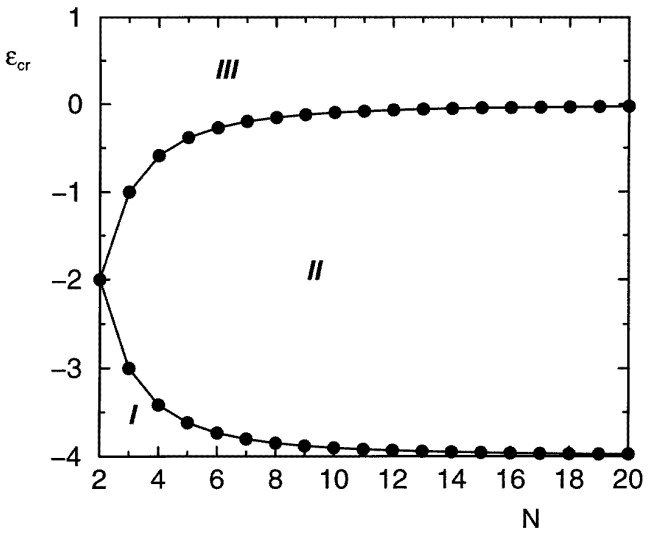

Figure 1. The phase diagram showing the critical ϵ_{cr}-values as functions of the block size N.

The previous analysis can be extended to the general case of an N-mer (two values ϵ_1 and ϵ_2 appear in blocks of length N) where the resonant energy is defined through the following condition:

$$\mu_N = \frac{\pi}{N}, \frac{2\pi}{N}, \frac{3\pi}{N}, \frac{4\pi}{N}, \cdots, \frac{(j+1)\pi}{N} \qquad j = 0, 1, 2, \ldots, N-2. \tag{5}$$

We note that as the block size N increases, the number of resonant states proportional to $2(N-1)$ increases as well. In the first zone, in particular, the disorder strength should be smaller than a critical strength $\epsilon_{cr}(N)$ for this to happen. The latter is obtained through the equation $2\cos(q_{cr}) + \epsilon_{1,2}\sin(q_{cr})/q_{cr} = 2\cos\mu_N$ that gives the corresponding critical wavevectors. Equivalently, ϵ_{cr} is obtained through

$$\frac{\sin q}{\cos q - \cos\mu_N} = -\frac{2q}{\epsilon_{cr}}. \tag{6}$$

The resonances inside the first band appear whenever the derivative of the left-hand side of equation (6) at $q = 0$ is less than $-2/\epsilon_{cr}$, and thus

$$\epsilon_{cr}(N) = 2(\cos(\mu_N) - 1). \tag{7}$$

In the phase diagram of figure 1 we distinguish three regions: region I, which contains no resonant states; region II, where some resonant states appear; and region III, where all resonant states are concentrated. The borders of region II start at $\epsilon = -2$ for $N = -2$ (the RDKP case) and are given by the curve for equation (7) with $\mu_N = \pi/N$ (upper bound) and $\mu_N = (N-1)\pi/N$ (lower bound), and approach zero and -4 respectively as $N \to \infty$. We recall that for the perfect Kronig–Penney lattice the range of accessible ϵ-values within the first energy band is $[-4, +\infty)$. We further note that the lower border corresponds to the existence of only one resonant state, while as we are going towards the upper border more resonances appear. The upper critical curve delimits region III in which all system resonances are found.

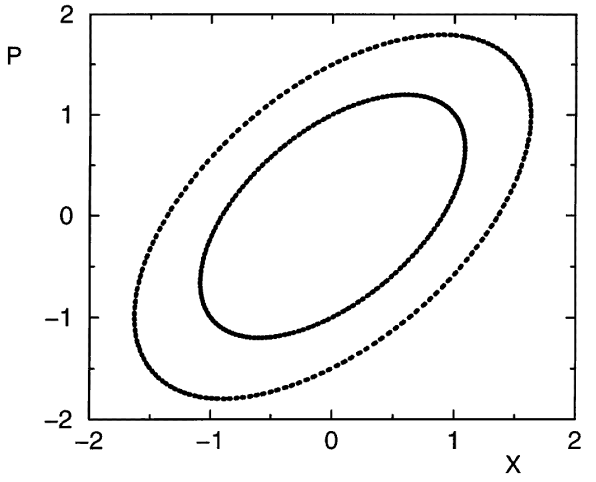

(a)

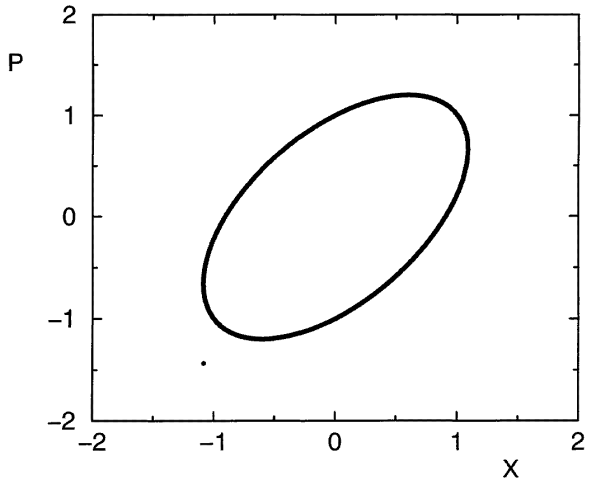

(b)

Figure 2. The phase space of the map of equation (13) for $p_0 = x_0 = 1$. (a) One value of ϵ_2 in the sequence ϵ: $\cdots\epsilon_1\epsilon_1\epsilon_1\epsilon_2\epsilon_1\epsilon_1\epsilon_1\cdots$ for $q_{cr} = 11.4$; $\epsilon_1 = 0$; $\epsilon_2 = 9.758\,85$. (b) Two values of ϵ_2 (one dimer) in the sequence ϵ: $\cdots\epsilon_1\epsilon_1\epsilon_1\epsilon_2\epsilon_2\epsilon_1\epsilon_1\epsilon_1\cdots$ for $\epsilon_1 = 0$; $\epsilon_2 = 9.758\,85$; $q_{cr} = 11.4$. We note that there is a point outside the ellipse representing the kick to the ϵ_1-trajectory by the first ϵ_2-value. The second ϵ_2-value kicks the trajectory back to the ellipse. (c) Dimers of type ϵ_2, randomly (with probability $Q = 0.5$) distributed in the sequence ϵ for $\epsilon_1 = 0$, $\epsilon_2 = 9.758\,85$ and $q_{cr} = 11.4$.

By introducing a new variable $p_{n+1} = x_{n+1} - x_n$ playing a role similar to momentum, we obtain through equation (3) a new map representation:

$$\begin{aligned} p_{n+1} &= p_n + f_n x_n \\ x_{n+1} &= x_n + p_{n+1} \end{aligned} \tag{8}$$

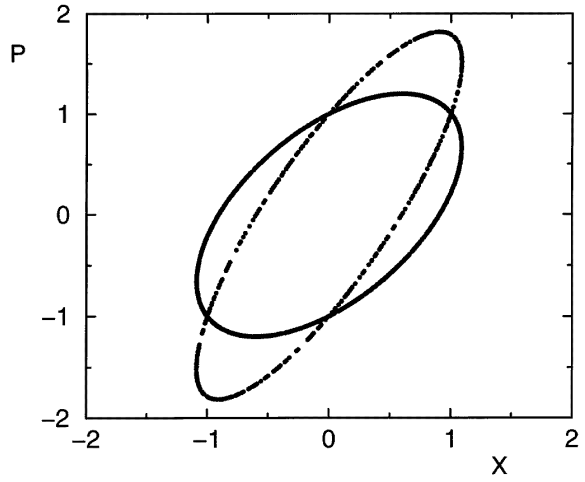

(c)

Figure 2. (Continued)

where $f_n = v_n - 2$ and has the same eigenvalues as the original map (3). In the map of equation (8), ellipses correspond to $\epsilon_n = \epsilon_1$ for all n, and a defect at site m with $\epsilon_m = \epsilon_2$ results in a kick into another ellipse (figure 2(a)), while correlated defects lead to a return to the original ellipse, since the total phase advance $\mu = \mu_m + \mu_{m+1} = \pi$ (figure 2(b)). When a random mixture of dimers with energy ϵ_2 is embedded in a chain with energy ϵ_1, we obtain a phase-space trajectory similar to the one in figure 2(c). We observe two ellipses corresponding to ϵ_1- and ϵ_2-values respectively. The second ellipse is formed by points occurring every time the first site of a dimer is encountered by the map. In the general case of a correlated M-block under the condition that the total sum $\sum_{n=1}^{M} \mu_n$ of phase shifts is equal to $m\pi$, for any sequence with m integer, the trajectory always returns to the ellipse associated with the 'perfect' sites to the left and to the right of the scattering potential.

2.2. The parametric linear oscillator

Another useful representation of the original model of equation (2), similar to the map of equation (8) but more convenient for the analysis of the localization length, can be obtained through two successive maps [9]:

$$\begin{aligned} \tilde{p}_n &= p_n + A_n x_n \\ \tilde{x}_n &= x_n \end{aligned} \tag{9}$$

and

$$\begin{aligned} p_{n+1} &= \tilde{p}_n \cos\mu_0 - \tilde{x}_n \sin\mu_0 \\ x_{n+1} &= \tilde{p}_n \sin\mu_0 + \tilde{x}_n \cos\mu_0. \end{aligned} \tag{10}$$

When the maps of equation (9) and equation (10) are combined, the result is a form of equation (2), namely

$$x_{n+1} + x_{n-1} = (2\cos\mu_0 + A_n \sin\mu_0)x_n. \tag{11}$$

Comparing with equation (2), one can establish the correspondences $\mu_0 = q$ and $A_n = \epsilon_n/q$ between the parameters q and ϵ_n in the original model (2), and the parameters μ_0 and A_n of the map of equations (9) and (10). The latter map has a clear meaning since the map of equation (9) corresponds to an instant linear kick of the strength A_n resulting in the change of the momentum p_n, and the map of equation (10) describes free rotation in the phase plane (p, x) defined by the angle μ_0. The dynamical system modelled by equations (9) and (10) is that of a linear oscillator with a periodic parametrical perturbation with a Hamiltonian [9]

$$\tilde{H} = \frac{\mu_0 p^2}{2} + \frac{\mu_0 x^2}{2} - \frac{1}{2}x^2\tilde{\delta}_1(t) \qquad \tilde{\delta}_1(t) \equiv \sum_{n=-\infty}^{\infty} A_n \delta(t-n). \tag{12}$$

We note that by integrating equation (1) between two successive δ-kicks of the potential, we obtain equation (10), while integration over a kick leads to equation (9) with a new kick strength $A_n = \epsilon_n$. By comparing equation (1) with equations (9) and (10) we find the significance of the variable p_n: it is the rescaled (with respect to $q = \sqrt{E}$) first derivative of the local amplitude function ϕ just before the nth kick, i.e. $p_n = (\mathrm{d}\phi/\mathrm{d}z)_{z=z_n}/q$.

For the dimer case defined by the two values of ϵ_1, ϵ_2, we can set without loss of generality $\epsilon_1 = 0$. As a result, the motion corresponding to $\epsilon_n = \epsilon_1$ is represented by the circle in the phase plane (p, x), and resonant behaviour results when, after a given number of kicks with $\epsilon_n = \epsilon_2$, the trajectory returns to this circle. An example of this behaviour is given in figure 3(a) for $q = q_{cr} = 11.4$ and $\epsilon_2 = 9.758\,85$. A similar behaviour for the case of a trimer, $N = 3$, is illustrated in figure 3(b) for $\epsilon_2 = 1.25$ and $q = q_{cr} = 1.489$. We observe that the trajectory is bounded in the phase space.

The above scheme is also valid for the much more general case where the locations of the δ-functions z_n in the original model, equation (1), are not equidistant and can be taken from an arbitrary distribution. In this case equation (10) has the same form provided that we make the substitution $\mu_0 \to \mu_{T_n} = qT_n$, where T_n corresponds to random periods of the kicks in the Hamiltonian approach (12). In the original model of equation (1), T_n indicates the random distance between two successive lattice sites, i.e. $T_n = z_{n+1} - z_n$. The critical value q_{cr} for the dimer is obtained directly from equation (11) using the relation $2\cos\mu_N = 2\cos\mu_{T_n} + A_n \sin\mu_{T_n}$ with $\mu_N = \pi/2$ (see equation (5)). As a result, we obtain $\tan(q_{cr}T_n) = -\epsilon/(2q_{cr})$ where both T_n and ϵ_n are related to the same lattice site z_n as in equation (1). Therefore, we conclude that in the case of a generalized dimer where time displacements T_n and the on-site potential are paired in such a way that $T_n = T_{n+1} = T_2$ and $\epsilon_n = \epsilon_{n+1} = \epsilon_2$, the condition for the critical energy will be similar to the one obtained previously, but with the change $\mu_0 \to \mu_{T_n} = \mu_2 = qT_2$.

2.3. Nearly resonant states

The representation of the model of equation (2) used in section 2.2 allows for the study of global properties of eigenstates. In particular, the resonant delocalized states correspond to a bounded motion described by the maps of equations (8), (9) and (10). Localized states on the other hand are represented by unbounded trajectories that escape from the origin of phase space (p, x). This is illustrated in figure 4 for the case of random dimers with non-resonant values of q. The exponential increase of a distance from the origin ($p = x = 0$) is related to the localization length of the corresponding eigenstate. In order to study the dependence of the localization length l for nearly resonant states, it is useful to pass to action-angle variables (r, θ) for the map of equations (9) and (10) using the definitions $x = r\cos\theta$ and

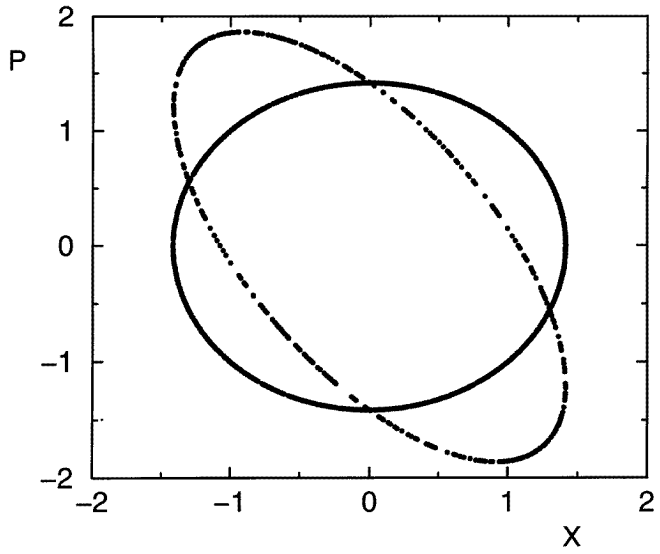

(a)

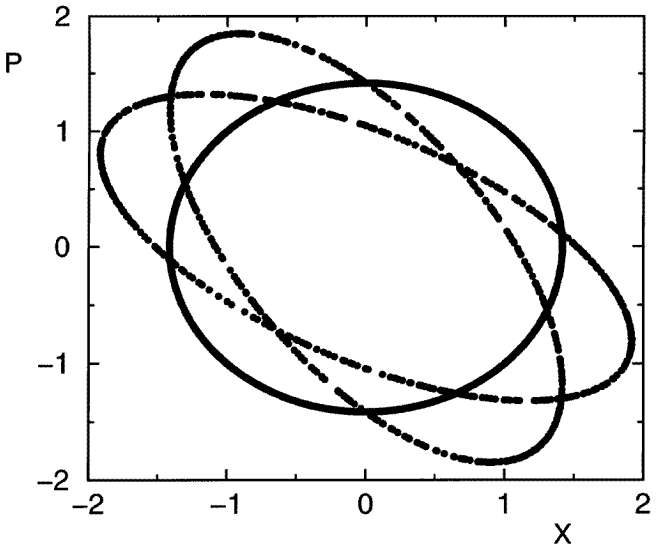

(b)

Figure 3. The phase space of the map of (16) and (17) for $p_0 = x_0 = 1$ and $Q = 0.5, \epsilon_1 = 0$. (a) $N = 2$ (dimer); $q_{cr} = 11.4$; $\epsilon_2 = 9.778\,85$. (b) $N = 3$ (trimer); $q_{cr} = 1.489$; $\epsilon_2 = 1.25$. The length of sequence ϵ is equal to $L = 1000$.

$p = r \sin\theta$. We obtain a map for the action r given by

$$r_{n+1}^2 = r_n^2 D_n^2 \qquad D_n^2 = (1 + A_n^2 \cos^2\theta_n + A_n \sin 2\theta_n) \tag{13}$$

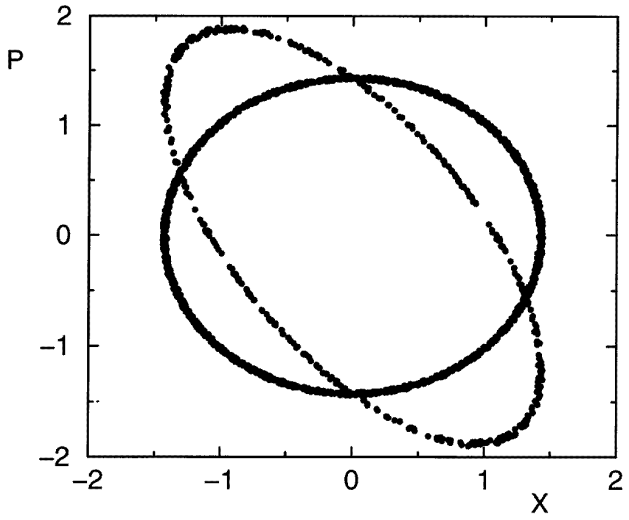

(a)

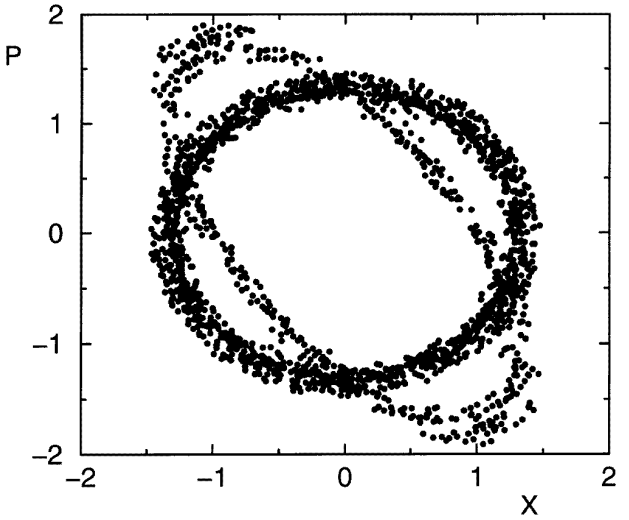

(b)

Figure 4. Nearly resonant states for a dimer ($N = 2$). Comparing with the resonant states shown in figures 2(c) and 3(a), nearly resonant states correspond to the unbounded (for $t \to \infty$) motion with a slow spread of the points in the phase space. (a) $q = 11.399$; $\epsilon_2 = 9.758\,85$. (b) $q = 11.390$; $\epsilon_2 = 9.758\,85$. (c) $q = 11.38$; $\epsilon_2 = 9.758\,85$.

where the transformation for $\cos\theta_n$ and $\sin\theta_n$ is given by the relations

$$\begin{aligned} \cos\theta_{n+1} &= D_n^{-1}\{\cos(\theta_n + \mu_0) - A_n \cos\theta_n \sin\mu_0\} \\ \sin\theta_{n+1} &= D_n^{-1}\{\sin(\theta_n + \mu_0) + A_n \cos\theta_n \cos\mu_0\}. \end{aligned} \tag{14}$$

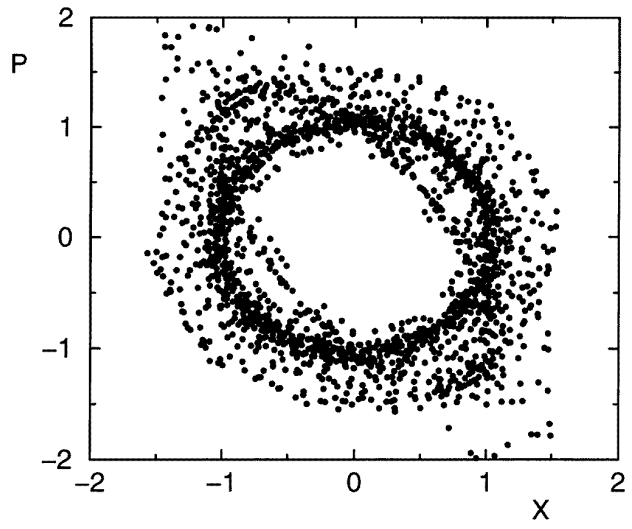

(c)

Figure 4. (Continued)

The relations of equations (13) and (14) can be used instead of the common transfer-matrix approach for the determination of the localization length l. The latter is equal to the inverse of the Lyapunov exponent γ defined as

$$\gamma = \lim_{N\to\infty} \frac{1}{N} \sum_{n=0}^{N-1} \ln\left(\frac{r_{n+1}}{r_n}\right) \tag{15}$$

where the ratio $r_{n+1}/r_n = D_n$ is given by (13).

The advantage of this approach in the finding of the Lyapunov exponent γ, in comparison to the standard transfer-matrix method, is that there is no divergence during iterations. It is interesting to note that equations (13) and (14) can be mapped onto a one-dimensional map $\theta_{n+1} = F(\theta_n)$ which is non-linear for the non-zero perturbation $A_n \neq 0$. One can show that in such a representation, the expression (13) is directly related to the stretching of the phase, $\mathrm{d}\theta_{n+1}/\mathrm{d}\theta_n = D_n^2$. Therefore, the original quantum problem is reduced to the study of the properties of a one-dimensional time-dependent map and its tangent space.

Due to correlations in the sequence θ_n, the expression (15) cannot be evaluated directly. However, it is possible to construct an effective map for two successive kicks of the single map (13) and neglect the correlations between the phases θ_{n+2} and θ_n near the resonance $q = q_{cr} - \delta \approx q_{cr}$. Applying the resulting two-step map [9] to the present case allows us to estimate the Lyapunov exponent for $\delta \ll 1$, using the expansion in $W = A_n\delta/\sin\mu_0$, with successive averaging over θ_n, leading to

$$\gamma \approx Q\frac{\delta^2\epsilon_2^2}{\mu_0^2\sin^2\mu_0}. \tag{16}$$

The factor Q stands for the probability for a dimer of the second kind (with energy ϵ_2) to appear. In figure 5 we compare the analytical result (16) (solid line) with the numerical data obtained from the map of (13) and (14) (circles) after iterating up to 4000 000 time steps and averaging over more than 1000 realizations of the random kick strengths A_n, for

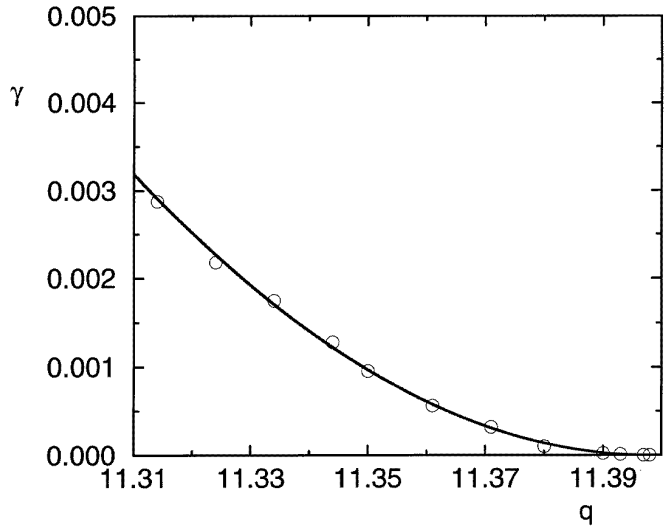

Figure 5. The numerical (circles) and analytical estimation (solid line) of the Lyapunov exponent for nearly resonant states. We use $q_{cr} = 11.4$. We observe good agreement.

the case where $Q = 0.5, \epsilon = 9.758\,85$ and $q_{cr} = 11.4$. The agreement between the theory and numerical data is extremely good as seen in figure 5, verifying that expression (16) is valid for $\delta \ll 1$.

From equation (16) we determine the dependence of the inverse of the localization length for the near-resonant states, and the way in which it changes when the system parameters change. We note that the higher the order of the resonance, $q \gg 1$ (i.e. the higher k in $[(2k-1)\pi/2, (2k+1)\pi/2]$), the larger the localization length, and thus—it is expected—the better the transport properties. Such a behaviour of $l(q)$ is expected since for $q \gg 1$ the second term of v_n (where q appears in the denominator) in equation (2) becomes negligible, leading to a tight-binding equation with zero on-site potential. The localization length increases also when ϵ is decreased towards zero. This is easily comprehended since when $\epsilon_1 = \epsilon_2 = 0$ we recover the properties of the perfect lattice. Finally, as the concentration Q of dimers decreases, the value of the localization length for the near-resonant states increases.

3. Transport properties

In this section we examine the transport properties of our system by studying the behaviour of the transmission coefficient. We assume that the system of equation (2) is a sample consisting of L lattice points with two identical semi-infinite perfect leads on either side. As a result, the left-hand lead extends over the range $-\infty < n \leqslant 0$, the sample extends over the range $1 \leqslant n \leqslant L$, and the right-hand lead extends over the range $L+1 < n < \infty$. The purpose of these leads is to carry the incoming, the reflected and the transmitted waves. Here E (see equation (1)) is the Fermi energy, and without any loss of generality we choose $\epsilon_n = 0$ everywhere in the leads.

In order to calculate the transmission amplitude t_L of a segment containing L sites we

inject a particle from $-\infty$ with an energy $\tilde{E} = 2\cos q$ towards the sample. While the particle passes through the sample it undergoes multiple elastic scattering. Eventually, it comes out of the sample from the right-hand end with amplitude t_L. Following Pichard [12] we write the transmission coefficient $T_L = |t_L|^2$ in terms of the matrix elements of the total transfer matrix $P_L = \prod_{n=1}^{L} M_n$ as

$$T_L = \frac{4|\sin q|^2}{|(P_L)_{21} - (P_L)_{12} + (P_L)_{22}\mathrm{e}^{\mathrm{i}q} - (P_L)_{11}\mathrm{e}^{-\mathrm{i}q}|^2}. \tag{17}$$

In the Hamiltonian map approach, the above system corresponds to the parametric linear oscillator of section 2.2 where the strength A_n of the instant linear kick (see equation (9)) is equal to zero for times $t \leqslant 0$ or $t \geqslant L + 1$ describing free rotations in the phase plane, while in the time interval $1 \leqslant t \leqslant L$ the strength A_n is determined by the disordered site energy ϵ_n of the underlying one-dimensional Schrödinger equation (1).

In order to establish a relation for the transmission coefficient in the framework of our Hamiltonian map approach, we recast the two successive maps of equations (9) and (10) as the following two-dimensional map Q_n:

$$\begin{pmatrix} x_{n+1} \\ p_{n+1} \end{pmatrix} = \begin{pmatrix} \cos\mu_0 + A_n \sin\mu_0 & \sin\mu_0 \\ A_n \cos\mu_0 - \sin\mu_0 & \cos\mu_0 \end{pmatrix} \begin{pmatrix} x_n \\ p_n \end{pmatrix} \tag{18}$$

which is related to the transfer matrix M_n defined in equation (3) through a similarity transformation R:

$$Q_n = RM_nR^{-1} \qquad R = \begin{pmatrix} 1 & 0 \\ \cos\mu_0/\sin\mu_0 & -1/\sin\mu_0 \end{pmatrix}. \tag{19}$$

From the above equation (19) and equation (17), one obtains for the transmission coefficient T_L of a system with L scatterers:

$$T_L = \frac{4}{((F_L)_{11}^2 + (F_L)_{21}^2) + ((F_L)_{12}^2 + (F_L)_{22}^2) + 2} \tag{20}$$

where the matrix F_L is the product transfer matrix, i.e $F_L = \prod_{n=1}^{L} Q_n$. From equation (20) we see that the sum inside the first parentheses in the denominator is equal to the inner product of the vector

$$v(t = L) = F_L \begin{pmatrix} 1 \\ 0 \end{pmatrix}$$

i.e., to the modulus squared of the vector

$$v(0) = \begin{pmatrix} 1 \\ 0 \end{pmatrix}$$

evolved under the dynamical map (18) (or equivalently under the map of (9) and (10)) for time $t = L$, in the phase space of the parametric linear oscillator described by the Hamiltonian (12). Similarly, the sum inside the second parentheses in the denominator in equation (20) corresponds to the modulus squared after the evolution for time $t = L$ of the initial vector

$$u(0) = \begin{pmatrix} 0 \\ 1 \end{pmatrix}.$$

It is interesting to note that the initial vectors $v(0), u(0)$ correspond to the unit vectors pointing in the two perpendicular directions on the phase-space plane.

Using these observations, we can give a geometrical interpretation for equation (20) namely that it relates T_L to areas in the phase space of the two-dimensional Hamiltonian

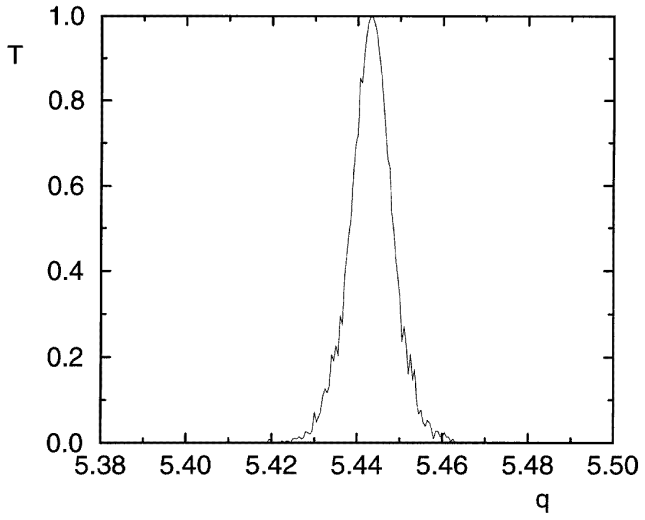

(a)

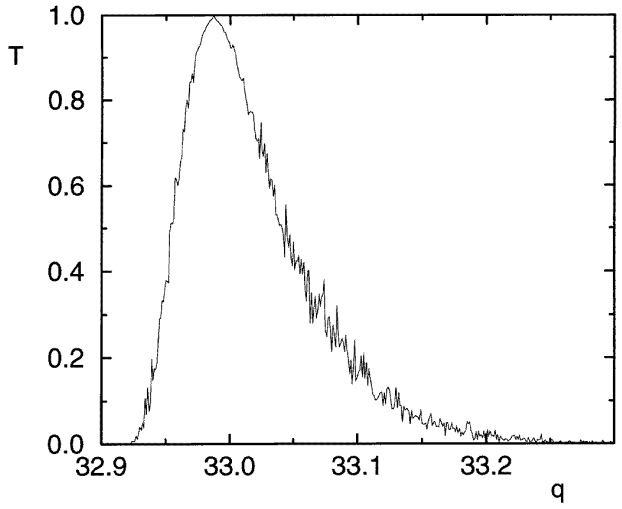

(b)

Figure 6. The transmission coefficient (averaged over more than 10 000 realizations) as a function of $q = E^2$ for a system with $\epsilon_1 = 0$, $\epsilon_2 = 9.758\,85$. (a) $Q = 0.5$ and $q_{cr} = 5.44$, corresponding to a resonance inside the second band. (b) $Q = 0.5$ and $q_{cr} = 33.13$, corresponding to a resonance inside the tenth energy band. We note that with respect to (a) the band of states with $T \approx 1$ is wider. (c) $Q = 0.2$ and $q_{cr} = 5.44$, corresponding to a resonance inside the second energy band. We note that with respect to (a) we now have more states with $T \approx 1$.

map (12). In particular, we can interpret the sum inside each set of parentheses in the denominator as the area of a circle described by a radius r_1, r_2 which is given by the time evolution (under the map (18)) of the initial vectors $(r_{1,2}, \theta_{1,2})_{t=0} = (1, 0), (1, \pi/2)$. Thus

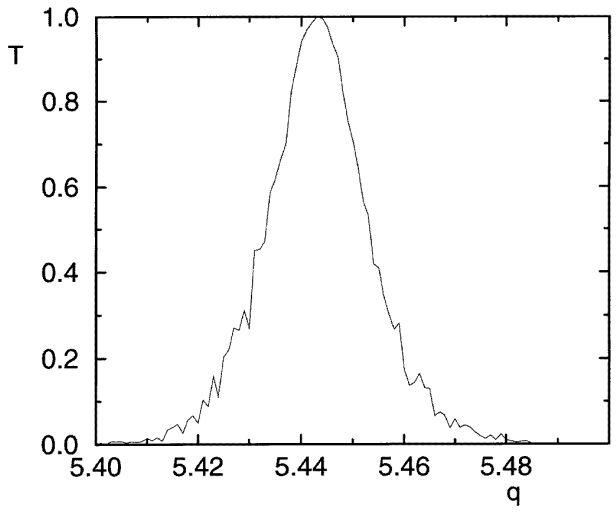

(c)

Figure 6. (Continued)

equation (20) can be rewritten in the following form:

$$T_L = \frac{4\pi}{\pi r_1^2 + \pi r_2^2 + 2\pi} = \frac{2S_{tot}^0}{S_{tot}^0 + S_{tot}^L} \tag{21}$$

where $S_{tot}^L = S_1^L + S_2^L$ is the sum of the areas defined by the radius r_1, r_2 at time $t = L$. In the case of a perfect lattice where we have simple rotations of the initial vectors $(r_{1,2}, \theta_{1,2})^0$, the areas defined after time L will be the same: $S_{tot}^L = S_{tot}^0 = 2\pi$, and hence $T_L = 1$.

Using equation (13) we can write equation (21) in a way that it is more tractable for numerical calculations, i.e.

$$T_L = 4 \Big/ \left(\prod_{n=0}^{L-1} (D_n^{(1)})^2 + \prod_{n=0}^{L-1} (D_n^{(2)})^2 + 2 \right) \tag{22}$$

where the $D^{i=1,2}$ correspond to the initial conditions $(r_i, \theta_i)^0 = (1, 0), (1, \pi/2)$ respectively.

The results that we have obtained so far provide an exact, although non-closed, analytical description of any one-dimensional system that can be written in the tight-binding form of equation (2). We will now evaluate them for the specific case of RDKP to describe those relevant features of the transmission coefficient that may be the fingerprint of extended states.

In figures 6(a) and 6(b) we show the numerical results for a system of 10 000 scatterers after averaging over more than 10 000 different realizations of the disordered sample. We take the values of $\epsilon_1 = 0$ and $\epsilon_2 = 9.758\,85$ and the defect concentration $Q = 0.5$, i.e. the most random case. In figure 6(a) we used the critical energy $q_{cr} = 5.443\,223$ lying inside the second zone of the spectrum, while in figure 6(b) we used $q_{cr} = 33.13$ lying inside the tenth zone. We note that states close to the resonant energies have very good transmission properties, similar to those at the resonant energy where the transmission coefficient T is equal to one. This is compatible with the findings of the random-dimer model with one band (the tight-binding approximation) [8]. Moreover, in the RDKP model, the width of the

peaks depends on the order of the resonance, as mentioned previously (see also [10]). From the comparison between figure 6(a) and figure 6(b) we see that the higher the resonance, the wider the band of states with $T \approx 1$. In figure 6(c) we present results for a different defect concentration Q in order to study the dependence of the transmission coefficient on Q. We use the same values of ϵ_1 and ϵ_2, and $Q = 0.2$. By comparison with figure 6(a) we conclude that as Q decreases the number of transparent states, i.e states with transmission coefficients close to one, $T \sim 1$, increases, in perfect agreement with the results of the previous section for the localization length of nearly resonant states.

4. Conclusions

We have studied a Kronig–Penney model with binary on-site disorder randomly assigned to every second site. For such a model it was found [10] that there exist an infinite number of special energies $E_{cr} = q_{cr}^2$ at which transparent states appear. We recover these results using a new approach based on classical Hamiltonian maps. We have generalized our results for a N-mer case, and obtained a simple expression for the resonant energy values. We constructed a phase diagram in the ϵ_{cr}–N plane which exhibits three distinct regions: one where no resonant states appear; a second that contains some of the resonant states; and a third that contains all possible resonant states for different correlated blocks of size N. This separation into three distinct regions is valid only in the first zone, and as a result it might have some relevance to the low-temperature system properties. Our dynamical system approach maps resonant delocalized states to bounded trajectories, while localized states are represented by unbounded trajectories in the phase space (p, x). Making use of an expansion in the vicinity of the resonance, we derived an analytical expression of equation (16) for the Lyapunov exponent for the nearly resonant states. Finally, in the framework of our Hamiltonian map we established a simple geometrical picture for the transmission coefficient showing that it corresponds to the evolution of areas in the phase space of a linear parametric oscillator. Using these last results we calculated the transmission coefficient that exhibits peaks up to $T = 1$ for energy values equal to the resonant ones. Near the resonant energies there are nearly transparent states with large transmission coefficients, the number of which is inversely proportional to the defect concentration Q and increases with the resonance order. The properties of the RDKP model that were analysed in this work could be used in mesoscopic quasi-one-dimensional studies.

Acknowledgments

We acknowledge the support of a ΠΕΝΕΔ 95-115 grant of the General Secretariat for Research and Technology of Greece. One of the authors (FMI) wishes to acknowledge the support of the Grant ERBCHRXCT 930331 from the Human Capital and Mobility Network of the European Community, and the support of Grant No RB7000 from the International Science Foundation. TK acknowledges with thanks many useful discussions on Anderson localization with A Politi during his visits to the Istituto Nazionale di Ottica.

References

[1] Dunlap D, Wu H-L and Phillips P 1990 *Phys. Rev. Lett.* **65** 88
[2] Phillips P and Wu H-L 1991 *Science* **252** 1805
[3] Bovier A 1992 *J. Phys. A: Math. Gen.* **25** 1021
[4] Flores J C 1989 *J. Phys.: Condens. Matter* **1** 8471

[5] Gangopadhyay S and Sen A K 1992 *J. Phys.: Condens. Matter* **4** 9939
[6] Evangelou S N and Economou E N 1993 *J. Phys. A: Math. Gen.* **26** 2803
[7] Evangelou S N and Wang A Z 1993 *Phys. Rev.* B **47** 13 126
[8] Datta P K, Giri D and Kundu K 1993 *Phys. Rev.* B **47** 10 727
Datta P K, Giri D and Kundu K 1993 *Phys. Rev.* B **48** 16 347
[9] Izrailev F M, Kottos T and Tsironis G P 1995 *Phys. Rev.* B **52** 3274
Izrailev F M, Kottos T and Tsironis G P 1996 *J. Phys.: Condens. Matter* **8** 2823
[10] Sánchez A, Maciá E and Domínguez-Adame F 1994 *Phys. Rev.* B **49** 147
[11] Bellissard J, Formoso A, Lima R and Testard D 1982 *Phys. Rev.* B **26** 3024
[12] Pichard J L 1986 *J. Phys. C: Solid State Phys.* **19** 1519